

Q^2 Dependence of Quadrupole Strength in the $\gamma^* p \rightarrow \Delta^+(1232) \rightarrow p\pi^0$ Transition

K. Joo,¹ L. C. Smith,¹ V. D. Burkert,³ R. Minehart,¹ I. G. Aznauryan,⁴ L. Elouadrhiri,^{2,3} S. Stepanyan,^{4,23} G. S. Adams,²⁴ M. J. Amarian,⁴ E. Anciant,²⁶ M. Anghinolfi,¹⁵ D. S. Armstrong,⁸ B. Asavapibhop,²⁹ G. Audit,²⁶ T. Auger,²⁶ H. Avakian,¹⁴ S. Barrow,¹² H. Bagdasaryan,⁴ M. Battaglieri,¹⁵ K. Beard,¹⁸ M. Bektasoglu,²³ W. Bertozzi,²⁰ N. Bianchi,¹⁴ A. S. Biselli,²⁴ S. Boiarinov,¹⁶ B. E. Bonner,²⁵ W. K. Brooks,³ J. R. Calarco,³⁰ G. P. Capitani,¹⁴ D. S. Carman,²² B. Carnahan,⁷ P. L. Cole,³⁴ A. Coleman,⁸ D. Cords,³ P. Corvisiero,¹⁵ D. Crabb,¹ H. Crannell,⁷ J. Cummings,²⁴ E. De Sanctis,¹⁴ R. De Vita,¹⁵ P. V. Degtyarenko,³ R. A. Demirchyan,⁴ H. Denizli,³¹ L. C. Dennis,¹² A. Deppman,¹⁴ K. V. Dharmawardane,²³ K. S. Dhuga,¹³ C. Djalali,³³ G. E. Dodge,²³ D. Doughty,^{2,3} P. Dragovitsch,¹² M. Dugger,⁵ S. Dytman,³¹ M. Eckhause,⁸ Y. V. Efremenko,¹⁶ H. Egiyan,⁸ K. S. Egiyan,⁴ L. Farhi,²⁶ R. J. Feuerbach,⁶ J. Ficencic,³⁵ K. Fissum,²⁰ T. A. Forest,²³ H. Funsten,⁸ M. Gai,²⁸ V. B. Gavrilov,¹⁶ S. Gilad,²⁰ G. P. Gilfoyle,³² K. L. Giovanetti,¹⁸ P. Girard,³³ K. A. Griffioen,⁸ M. Guidal,¹⁷ M. Guillo,³³ V. Gyurjyan,³ D. Hancock,⁸ J. Hardie,² D. Heddle,^{2,3} J. Heisenberg,³⁰ F. W. Hersman,³⁰ K. Hicks,²² R. S. Hicks,²⁹ M. Holtrop,³⁰ C. E. Hyde-Wright,²³ M. M. Ito,³ D. Jenkins,³⁵ J. H. Kelley,⁹ M. Khandaker,^{21,3} K. Y. Kim,³¹ W. Kim,¹⁹ A. Klein,²³ F. J. Klein,³ M. Klusman,²⁴ M. Kossov,¹⁶ Y. Kuang,⁸ S. E. Kuhn,²³ J. M. Laget,²⁶ D. Lawrence,²⁹ A. Longhi,⁷ K. Loukachine,³⁵ M. Lucas,³³ R. W. Major,³² J. J. Manak,³ C. Marchand,²⁶ S. K. Matthews,⁷ S. McAleer,¹² J. W. C. McNabb,⁶ B. A. Mecking,³ M. D. Mestayer,³ C. A. Meyer,⁶ M. Mirazita,¹⁴ R. Miskimen,²⁹ V. Muccifora,¹⁴ J. Mueller,³¹ G. S. Mutchler,²⁵ J. Napolitano,²⁴ G. Niculescu,²² B. Niczyporuk,³ R. A. Niyazov,²³ M. S. Ohandjanyan,⁴ A. Opper,²² Y. Patois,³³ G. A. Peterson,²⁹ S. Philips,¹³ N. Pivnyuk,¹⁶ D. Pocanic,¹ O. Pogorelko,¹⁶ E. Polli,¹⁴ B. M. Preedom,³³ J. W. Price,²⁷ L. M. Qin,²³ B. A. Raue,^{11,3} A. R. Reolon,¹⁴ G. Riccardi,¹² G. Ricco,¹⁵ M. Ripani,¹⁵ B. G. Ritchie,⁵ F. Ronchetti,¹⁴ P. Rossi,¹⁴ D. Rowntree,²⁰ P. D. Rubin,³² C. W. Salgado,²¹ M. Sanzone,¹⁴ V. Sapunenko,¹⁵ M. Sargsyan,⁴ R. A. Schumacher,⁶ Y. G. Sharabian,⁴ J. Shaw,²⁹ S. M. Shuvalov,¹⁶ A. Skabelin,²⁰ E. S. Smith,³ T. Smith,³⁰ D. I. Sober,⁷ M. Spraker,⁹ P. Stoler,²⁴ M. Taiuti,¹⁵ S. Taylor,²⁵ D. Tedeschi,³³ R. Thompson,³¹ L. Todor,⁶ T. Y. Tung,⁸ M. F. Vineyard,³² A. Vlassov,¹⁶ H. Weller,⁹ L. B. Weinstein,²³ R. Welsh,⁸ D. P. Weygand,³ S. Whisnant,³³ M. Witkowski,²⁴ E. Wolin,³ A. Yegneswaran,³ J. Yun,²³ Z. Zhou,²⁰ and J. Zhao²⁰

(The CLAS Collaboration)

¹University of Virginia, Department of Physics, Charlottesville, Virginia 22903

²Christopher Newport University, Newport News, Virginia 23606

³Thomas Jefferson National Accelerator Facility, 12000 Jefferson Avenue, Newport News, Virginia 23606

⁴Yerevan Physics Institute, 375036 Yerevan, Armenia

⁵Arizona State University, Department of Physics and Astronomy, Tempe, Arizona 85287

⁶Carnegie Mellon University, Department of Physics, Pittsburgh, Pennsylvania 15213

⁷Catholic University of America, Department of Physics, Washington D.C. 20064

⁸College of William and Mary, Department of Physics, Williamsburg, Virginia 23187

⁹Duke University, Physics Building TUNL, Durham, North Carolina 27706

¹⁰Department of Physics and Astronomy, Edinburgh University, Edinburgh EH9 3JZ, United Kingdom

¹¹Florida International University, Miami, Florida 33199

¹²Florida State University, Department of Physics, Tallahassee, Florida 32306

¹³George Washington University, Department of Physics, Washington, D.C. 20052

¹⁴Istituto Nazionale di Fisica Nucleare, Laboratori Nazionali di Frascati, P.O. 13, 00044 Frascati, Italy

¹⁵Istituto Nazionale di Fisica Nucleare, Sezione di Genova e Dipartimento di Fisica dell'Università, 16146 Genova, Italy

¹⁶Institute of Theoretical and Experimental Physics, 25 B. Cheremushkinskaya, Moscow, 117259 Russia

¹⁷Institut de Physique Nucleaire d'Orsay, IN2P3, BP 1, 91406 Orsay, France

¹⁸James Madison University, Department of Physics, Harrisonburg, Virginia 22807

¹⁹Kyungpook National University, Department of Physics, Taegu 702-701, South Korea

²⁰M.I.T.-Bates Linear Accelerator, Middleton, Massachusetts 01949

²¹Norfolk State University, Norfolk, Virginia 23504

²²Ohio University, Department of Physics, Athens, Ohio 45701

²³Old Dominion University, Department of Physics, Norfolk, Virginia 23529

²⁴Rensselaer Polytechnic Institute, Department of Physics, Troy, New York 12181

²⁵Rice University, Bonner Lab, Box 1892, Houston, Texas 77251

²⁶CEA Saclay, DAPNIA-SPhN, F91191 Gif-sur-Yvette Cedex, France

²⁷University of California at Los Angeles, Department of Physics and Astronomy, Los Angeles, California 90095-1547

²⁸University of Connecticut, Physics Department, Storrs, Connecticut 06269

²⁹University of Massachusetts, Department of Physics, Amherst, Massachusetts 01003

³⁰University of New Hampshire, Department of Physics, Durham, New Hampshire 03824

³¹University of Pittsburgh, Department of Physics and Astronomy, Pittsburgh, Pennsylvania 15260

³²University of Richmond, Department of Physics, Richmond, Virginia 23173

³³University of South Carolina, Department of Physics, Columbia, South Carolina 29208

³⁴University of Texas at El Paso, Department of Physics, El Paso, Texas 79968

³⁵Virginia Polytechnic and State University, Department of Physics, Blacksburg, Virginia 24061

(Received 2 October 2001; published 6 March 2002)

Models of baryon structure predict a small quadrupole deformation of the nucleon due to residual tensor forces between quarks or distortions from the pion cloud. Sensitivity to quark versus pion degrees of freedom occurs through the Q^2 dependence of the magnetic (M_{1+}), electric (E_{1+}), and scalar (S_{1+}) multipoles in the $\gamma^* p \rightarrow \Delta^+ \rightarrow p\pi^0$ transition. We report new experimental values for the ratios E_{1+}/M_{1+} and S_{1+}/M_{1+} over the range $Q^2 = 0.4\text{--}1.8$ GeV², extracted from precision $p(e, e'p)\pi^0$ data using a truncated multipole expansion. Results are best described by recent unitary models in which the pion cloud plays a dominant role.

DOI: 10.1103/PhysRevLett.88.122001

PACS numbers: 13.60.Le, 13.40.Gp, 14.20.Gk

Electroproduction of nucleon resonances provides unique information about the internal dynamics of baryons. For the $\gamma^* N \rightarrow \Delta(1232) \rightarrow N\pi$ transition, a long-standing problem is to achieve a consistent experimental and theoretical description of the electric and scalar quadrupole multipoles E_{1+} and S_{1+} , and the magnetic dipole M_{1+} . Within SU(6) models this transition is mediated by a single quark spin flip in the $L = 0$ nucleon ground state, leading to M_{1+} dominance and $E_{1+} = S_{1+} \equiv 0$. QCD-motivated constituent quark models introduce a tensor force from the interquark hyperfine interaction, which leads to a d -state admixture in the baryon wave function [1]. As a result small but nonzero values for E_{1+} and S_{1+} are predicted [1,2]. Stronger contributions are expected from the pion cloud [3–6] or from two-body exchange currents [7]. Finally, quark helicity conservation in perturbative QCD (pQCD) requires $E_{1+} = M_{1+}$ as $Q^2 \rightarrow \infty$.

Determination of the ratios $R_{EM} = E_{1+}/M_{1+}$ and $R_{SM} = S_{1+}/M_{1+}$ has been the aim of a considerable number of experiments in the past. While theoretical models have become more refined, most previous measurements have large systematic and statistical errors or significantly limited kinematic coverage. A new program using the CEBAF Large Acceptance Spectrometer (CLAS) [8] at Jefferson Lab has been inaugurated to vastly improve the systematic and statistical precision by covering a wide kinematic range of four-momentum transfer Q^2 and invariant mass W , and by subtending the full angular range of the resonance decay into the πN final state.

This Letter reports the first CLAS results for R_{EM} and R_{SM} obtained from a partial wave analysis of the $p(e, e'p)\pi^0$ reaction for $Q^2 = 0.4\text{--}1.8$ GeV². This Q^2 range explores distance scales where dynamical breaking of chiral symmetry may introduce collective degrees of freedom in the nucleon. Interest in chiral models recently increased after photopion measurements from LEGS [9] and MAMI [10] found $R_{EM} = -3.1\%$ and -2.5% , respectively, at $Q^2 = 0$, which is substantially larger than

constituent quark model predictions [1,2]. Chiral bag [3] and soliton models [4–6] in which quark confinement occurs through nonlinear interactions with the pion cloud, generally find R_{EM} in the range -1% to -5% at $Q^2 = 0$. Chiral effective field theories [11] and unitary [12] and dynamical reaction models [13,14] that employ pion rescattering at the $\gamma^* N\Delta$ vertex predict meson degrees of freedom should enhance the quadrupole strength at low Q^2 and strongly affect the Q^2 dependence of R_{EM} and R_{SM} .

Under the one-photon-exchange approximation, the pion electroproduction cross section factorizes as follows:

$$\frac{d^5\sigma}{dE_{e'}d\Omega_{e'}d\Omega_{\pi}^*} = \Gamma_{\nu} \frac{d^2\sigma}{d\Omega_{\pi}^*}, \quad (1)$$

where Γ_{ν} is the virtual photon flux. For an unpolarized beam and target the center-of-mass (c.m.) differential cross section $d^2\sigma/d\Omega_{\pi}^*$ depends on the transverse ϵ and longitudinal ϵ_L polarization of the virtual photon through four structure functions: σ_T , σ_L , and the interference terms σ_{LT} and σ_{TT} :

$$\begin{aligned} \frac{d^2\sigma}{d\Omega_{\pi}^*} = & \frac{p_{\pi}^*}{k_{\gamma}^*} [\sigma_T + \epsilon_L \sigma_L + \epsilon \sigma_{TT} \sin^2\theta_{\pi}^* \cos 2\phi_{\pi}^* \\ & + \sqrt{2\epsilon_L(\epsilon + 1)} \sigma_{LT} \sin\theta_{\pi}^* \cos\phi_{\pi}^*], \quad (2) \end{aligned}$$

where $(p_{\pi}^*, \theta_{\pi}^*, \phi_{\pi}^*)$ are the π^0 c.m. momentum, polar, and azimuthal angles, $\epsilon_L = (Q^2/|k^*|^2)\epsilon$, and $|k^*|$ and k_{γ}^* are the virtual photon c.m. momentum and real photon c.m. equivalent energy. A partial wave expansion of the structure functions using Legendre polynomials $P_l(\cos\theta_{\pi}^*)$ gives (for s and p waves)

$$\sigma_T + \epsilon_L \sigma_L = A_0 + A_1 P_1 + A_2 P_2, \quad (3a)$$

$$\sigma_{TT} = C_0, \quad (3b)$$

$$\sigma_{LT} = D_0 + D_1 P_1. \quad (3c)$$

The weak quadrupole E_{1+} and S_{1+} transitions are accessible only through their interference with the dominant M_{1+} . To simplify the analysis, a truncated multipole expansion is used, in which only terms involving M_{1+} are

retained. Thus, $|M_{1+}|^2$ and its projection onto the other s - and p -wave multipoles E_{1+} , S_{1+} , M_{1-} , E_{0+} , S_{0+} are given in terms of the six partial-wave coefficients by [15]

$$|M_{1+}|^2 = A_0/2, \quad (4a)$$

$$\text{Re}(E_{1+}M_{1+}^*) = (A_2 - 2C_0/3)/8, \quad (4b)$$

$$\text{Re}(M_{1-}M_{1+}^*) = -[A_2 + 2(A_0 + C_0)]/8, \quad (4c)$$

$$\text{Re}(E_{0+}M_{1+}^*) = A_1/2, \quad (4d)$$

$$\text{Re}(S_{0+}M_{1+}^*) = D_0, \quad (4e)$$

$$\text{Re}(S_{1+}M_{1+}^*) = D_1/6. \quad (4f)$$

In accordance with previous analyses [10,16] we define R_{EM} and R_{SM} as

$$R_{EM} = \text{Re}(E_{1+}M_{1+}^*)/|M_{1+}|^2, \quad (5)$$

$$R_{SM} = \text{Re}(S_{1+}M_{1+}^*)/|M_{1+}|^2. \quad (6)$$

Near the $\Delta(1232)$ mass, where the isospin 3/2 channel dominates and $\text{Re}(M_{1+}^{(3/2)})$ vanishes, $R_{EM} \approx \text{Im}(E_{1+}^{(3/2)})/\text{Im}(M_{1+}^{(3/2)})$ and similarly for R_{SM} . The contribution to R_{EM} from $\text{Re}(M_{1+}^{(1/2)})$ was estimated in [10] to be $<0.5\%$ absolute at $Q^2 = 0$, and is $<0.3\%$ for $Q^2 < 2.0 \text{ GeV}^2$ [12].

The present measurement used two beam energies (1.645 and 2.445 GeV) to cover the interval $Q^2 = 0.4\text{--}1.8 \text{ GeV}^2$. A 2.5 nA beam was delivered onto a 4.0 cm long liquid-hydrogen target at 100% duty factor. Particles were detected in CLAS, which provides momentum coverage down to 0.1 GeV/ c over a polar angle (θ) range $8^\circ\text{--}142^\circ$ and covers nearly 80% of the azimuthal angle ϕ . A hardware electron trigger was formed using threshold Čerenkov counters and electromagnetic calorimeters, while protons were identified using time-of-flight. Software fiducial cuts excluded regions of nonuniform detector response, and the acceptance and tracking efficiency were determined using a Monte Carlo simulation and a GEANT model of the detector. After kinematic corrections the invariant mass W resolution was $\sigma_W \approx 8\text{--}10 \text{ MeV}$.

Coincident protons were used to identify the π^0 . A typical missing mass spectrum is compared in Fig. 1 to

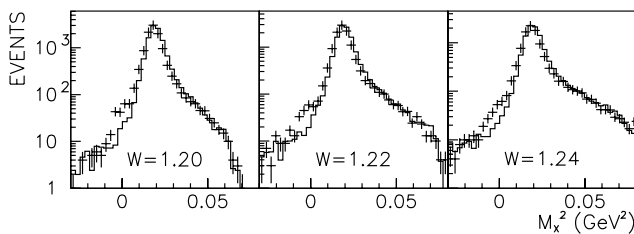


FIG. 1. Experimental $p(e, e'p)X$ missing mass for invariant mass W bins around the $\Delta(1232)$ (note logarithmic scale). Solid line: Simulation of CLAS response to $p(e, e'p)\pi^0$ reaction. The small shoulder at $M_x^2 = 0$ is due to residual $ep \rightarrow e'p\gamma$ events which survive the kinematic cuts.

a GEANT simulation that incorporates radiation effects and detector resolution, using a phenomenological model of the $p(e, e'p)\pi^0$ reaction. Good agreement with the width and radiative tail of the π^0 peak is seen. Background from elastic Bethe-Heitler radiation was suppressed using a combination of cuts on missing mass and ϕ_π^* near $M_x^2 = 0$ and $\phi_\pi^* = 0^\circ$. A cut of $-0.01 \leq M_x^2(\text{GeV}^2) \leq 0.08$ was used to select the $p\pi^0$ final state. Target window backgrounds and proton scattering from the torus coils were suppressed with cuts on the reconstructed $e'p$ target vertex.

Systematic errors in the electron kinematics, acceptance, and radiative corrections were determined by measuring inclusive (e, e') elastic and inelastic cross sections simultaneously with the exclusive data. The results agreed to within 5% with parametrizations of previous measurements. Determination of the $\pi^0 p$ c.m. angles (θ_π^* , ϕ_π^*) was affected by residual $ep \rightarrow e'p\gamma$ backgrounds, radiative and kinematic corrections, and proton multiple scattering. These systematic effects were estimated by varying cuts on missing mass, target vertex reconstruction, and fiducial acceptance. Model dependence of the acceptance and radiative corrections was studied in detail and included in the systematic error.

Typical cross sections obtained after radiative corrections are shown in Fig. 2 for $W = 1.22 \text{ GeV}$ and illustrate the complete out-of-plane ϕ_π^* coverage possible with CLAS. The presence of nonzero σ_{TT} and σ_{LT} strength is clearly indicated by the $\cos 2\phi_\pi^*$ and $\cos \phi_\pi^*$ modulation of the cross sections. These terms were separated from $\sigma_T + \epsilon_L \sigma_L$ by fitting the ϕ_π^* distributions with the form in Eq. (2). The extracted structure functions are shown in Fig. 3 for several W bins around the $\Delta(1232)$ peak. Fits to the $\cos \theta_\pi^*$ dependence using Eq. (3) are indicated by the solid curves. Inclusion of d waves, which would lead to deviations from the linear behavior for σ_{TT} and σ_{LT} in Fig. 3, did not improve the fit.

Figure 4 shows the W dependence of the partial wave coefficients obtained from the structure function fits. The data are compared to calculations of Drechsel *et al.* (MAID) [12] and Sato and Lee (SL) [13]. These models include unitarized contributions from Born diagrams and vector meson exchange, with the model parameters fitted

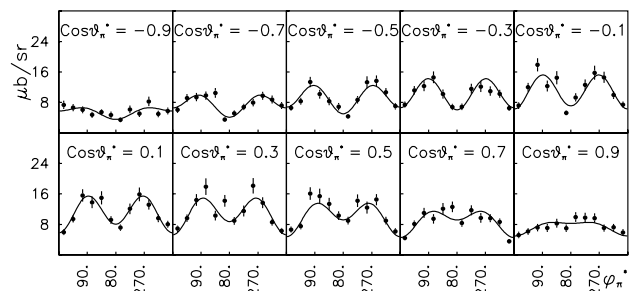


FIG. 2. Typical ϕ_π^* dependence for the $p(e, e'p)\pi^0$ cross sections at $Q^2 = 0.9 \text{ GeV}^2$ and $W = 1.22 \text{ GeV}$. Solid line: Fit to data according to Eq. (2). Errors are statistical only.

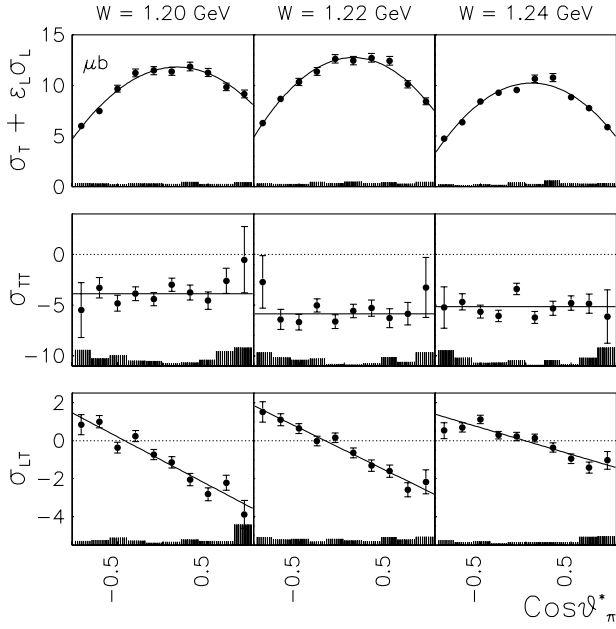


FIG. 3. Structure functions versus $\cos\theta_{\pi}^*$ extracted for the $p(e, e'p)\pi^0$ reaction at $Q^2 = 0.9 \text{ GeV}^2$. Solid line: Legendre polynomial fit to the data using Eq. (3). Shaded bars show systematic errors.

to previous photo- and electroproduction data. The curves show predicted contributions from all s - and p -wave multipoles. For the A_0 coefficient, which is dominated by the well-known $|M_{1+}|^2$, both SL and MAID describe the shape and magnitude quite well for $W < 1.26 \text{ GeV}$. The neglect of higher-mass resonances in the SL model is clearly evident for $W > 1.26 \text{ GeV}$. A_1 and D_0 are dominated by the interference between M_{1+} and the nonresonant electric and scalar s -wave multipoles E_{0+} and S_{0+} . Our results are clearly sensitive to differences between the models, which arise partly from the treatment of backgrounds.

The quadrupole interference terms $\text{Re}(E_{1+}M_{1+}^*)$ and $\text{Re}(S_{1+}M_{1+}^*)$ were extracted from the A_2 , C_0 , and D_1 coefficients using Eqs. (4b) and (4f), while $|M_{1+}|^2$ was determined using Eq. (4a). The ratios R_{EM} and R_{SM} were determined at $W = 1.20, 1.22, \text{ and } 1.24 \text{ GeV}$ and averaged to smooth statistical fluctuations. Errors arising from the M_{1+} dominance assumption and the averaging procedure were estimated by fitting “pseudo-data” generated from the MAID and SL models and binned identically to the CLAS data. The fitted terms were then compared to those calculated from the model input multipoles. Our typical(worst) absolute truncation error (including model dependence) was 0.3(0.7)% for R_{EM} and 0.1(0.5)% for R_{SM} over the Q^2 range of this experiment, with the error generally increasing with Q^2 due to the larger relative importance of neglected nonresonant multipoles. Results for each Q^2 bin are listed in Table I. Note that measurements at the same Q^2 but different beam energies agree within the uncertainties, lending credence to the accuracy of the corrections.

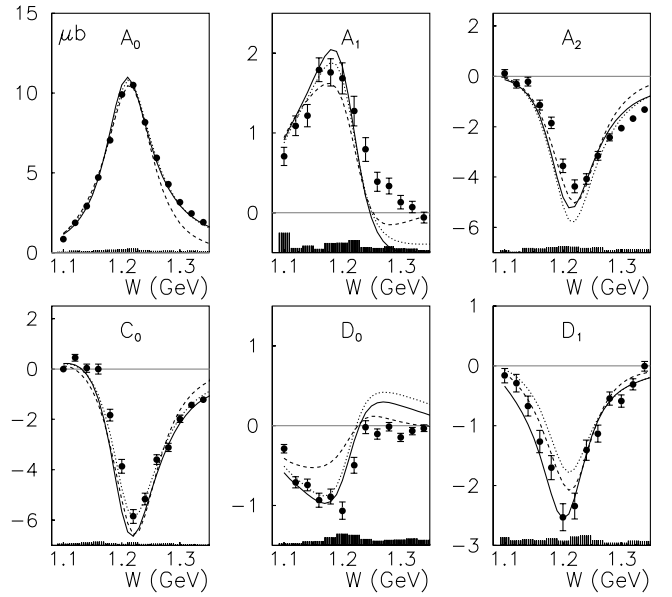


FIG. 4. W dependence of the Legendre coefficients obtained from structure function fits at $Q^2 = 0.9 \text{ GeV}^2$. The curves show model predictions (s - and p -wave multipoles only) from MAID98 [12] (dotted), MAID00 [17] (solid), and Sato-Lee [13] (dashed). Shaded bars show systematic errors.

Figure 5 summarizes the Q^2 dependence of the available R_{EM} and R_{SM} data compared to recent model calculations. Our results show no Q^2 dependence for R_{EM} , in contrast to the rapid falloff to zero predicted by chiral-quark/soliton models (χ QSM) [5,6]. Although motivated by chiral symmetry, these models ignore the $\Delta \rightarrow \pi N$ decay and rescattering effects. The two relativistic quark model R_{EM} curves, RQM1 [21] and RQM2 [22], agree at $Q^2 = 0$, but strongly diverge for $Q^2 > 0$, while the zero crossing seen in [22] is excluded by the CLAS data. Our overall $R_{EM} \approx -2\%$ is consistent with recent measurements both at lower Q^2 [9,10,18], and at higher Q^2 [16]. The Coulomb quadrupole ratio R_{SM} is significantly larger in magnitude and shows a strong Q^2 dependence. While the

TABLE I. Quadrupole/magnetic dipole ratios for the $\gamma^*N \rightarrow \Delta(1232)$ transition from partial wave fits at invariant momentum transfer Q^2 and beam energy E_e . The first error is statistical, while the experiment-related systematic effects are included in the second error.

Q^2 (GeV ²)	E_e (GeV)	$\text{Re}(E_{1+}/M_{1+})$ (%)	$\text{Re}(S_{1+}/M_{1+})$ (%)
0.40	1.645	$-3.4 \pm 0.4 \pm 0.4$	$-5.6 \pm 0.4 \pm 0.6$
0.52	1.645	$-1.6 \pm 0.4 \pm 0.4$	$-6.4 \pm 0.4 \pm 0.5$
0.65	1.645	$-1.9 \pm 0.5 \pm 0.5$	$-6.9 \pm 0.6 \pm 0.5$
0.75	1.645	$-2.1 \pm 0.6 \pm 0.7$	$-7.4 \pm 0.8 \pm 0.5$
0.90	1.645	$-1.8 \pm 0.6 \pm 0.4$	$-8.4 \pm 0.9 \pm 0.4$
0.65	2.445	$-2.0 \pm 0.4 \pm 0.4$	$-6.6 \pm 0.4 \pm 0.2$
0.75	2.445	$-1.6 \pm 0.5 \pm 0.5$	$-6.0 \pm 0.4 \pm 0.2$
0.90	2.445	$-1.8 \pm 0.4 \pm 0.3$	$-7.2 \pm 0.4 \pm 0.1$
1.15	2.445	$-1.6 \pm 0.5 \pm 0.3$	$-7.9 \pm 0.5 \pm 0.4$
1.45	2.445	$-2.4 \pm 0.7 \pm 0.4$	$-7.7 \pm 0.9 \pm 0.7$
1.80	2.445	$-0.9 \pm 1.1 \pm 0.7$	$-11.6 \pm 1.6 \pm 1.5$

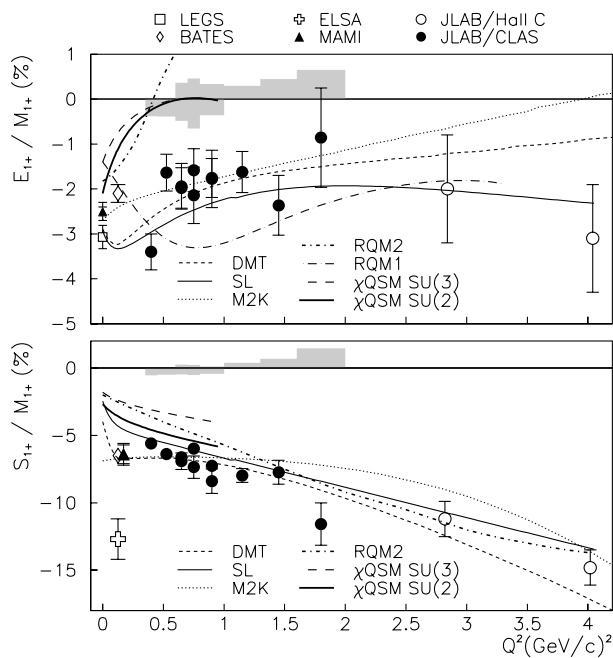


FIG. 5. Q^2 dependence of the electric (E_{1+}) and scalar (S_{1+}) quadrupole/magnetic dipole ratios from this experiment (\bullet). Shaded bands show systematic errors for the two beam energies listed in Table I. Truncation/averaging errors are discussed in the text. Other points are from BATES [18], ELSA [19], JLAB/Hall C [16], LEGS [9], and MAMI [10,20]. The curves show recent model calculations (see text): χ QSM [5], DMT [14], SL [13], M2K [14,17], RQM1 [21], and RQM2 [22].

chiral models and RQM2 do somewhat better in comparison with R_{SM} , so far no quark or chiral soliton model is able to successfully describe both R_{EM} and R_{SM} .

Dynamical pion rescattering models calculate a meson “dressed” $\gamma^*N\Delta$ vertex in terms of the underlying “bare” photocoupling form factors. Sato and Lee [13] fitted their dynamical model to photopion observables [10] and the JLAB/Hall C cross sections at $Q^2 = 2.8$ and 4.0 GeV^2 [16] using a common parametrization for the bare charge $G_C(Q^2)$ and electric $G_E(Q^2)N \rightarrow \Delta$ quadrupole form factors. Near $Q^2 = 0$, $G_C(0)$ was determined from $G_E(0)$ using the long wavelength limit (Siegert’s theorem). The SL curves shown in Fig. 5 describe the Q^2 trend of the CLAS data reasonably well. However, the SL model provides a poor fit to the BATES data [18] at $Q^2 = 0.126$ GeV^2 and the SL curve clearly misses the MAMI R_{SM} point [20]. Those data are better described by the Dubna-Mainz-Taipei (DMT) dynamical model [14] and a new version of MAID (M2K) [14,17] (also refitted to the high Q^2 data), both of which use different prescriptions for unitarization. Although the overall magnitude of the CLAS R_{EM} and R_{SM}

measurements is somewhat better described by DMT, our lowest Q^2 point marginally favors the SL prediction.

The generally successful description of both R_{EM} and R_{SM} by the dynamical models strengthens the claim made in [13,14] that nonresonant meson exchange dominates the $N \rightarrow \Delta(1232)$ quadrupole transition. This has important implications for the interpretation of pure quark model predictions of photocoupling amplitudes, where pion degrees of freedom are not explicitly treated. The low Q^2 evolution of E_{1+} and S_{1+} is especially important, since model independent constraints from Siegert’s theorem, gauge invariance, chiral perturbation theory [11], and ultimately lattice calculations can be most accurately applied in this region.

We acknowledge the efforts of the staff of the Accelerator and Physics Divisions at Jefferson Lab in their support of this experiment. This work was supported in part by the U.S. Department of Energy, including DOE Contract No. DE-AC05-84ER40150, the National Science Foundation, the French Commissariat à l’Energie Atomique, the Italian Istituto Nazionale di Fisica Nucleare, and the Korea Research Foundation.

- [1] N. Isgur, G. Karl, and R. Koniuk, Phys. Rev. D **25**, 2394 (1982).
- [2] S. Capstick and G. Karl, Phys. Rev. D **41**, 2767 (1990).
- [3] K. Bermuth *et al.*, Phys. Rev. D **37**, 89 (1988).
- [4] H. Walliser and G. Holzwarth, Z. Phys. A **357**, 317 (1997).
- [5] A. Silva *et al.*, Nucl. Phys. **A675**, 637 (2000).
- [6] L. Amoreira, P. Alberto, and M. Fiolhais, Phys. Rev. C **62**, 045202 (2000).
- [7] A. J. Buchmann *et al.*, Phys. Rev. C **58**, 2478 (1998).
- [8] W. Brooks, Nucl. Phys. **A663**, 1077 (2000).
- [9] G. Blanpied *et al.*, Phys. Rev. C **64**, 025203 (2001).
- [10] R. Beck *et al.*, Phys. Rev. C **61**, 035204 (2000).
- [11] G. Gellas *et al.*, Phys. Rev. D **60**, 054022 (1999).
- [12] D. Drechsel *et al.*, Nucl. Phys. **A645**, 145 (1999). <http://www.kph.uni-mainz.de/T/maid/maid.html>
- [13] T. Sato and T. S. H. Lee, Phys. Rev. C **63**, 055201 (2001).
- [14] Sabit S. Kamalov *et al.*, Phys. Rev. C **64**, 033201 (2001).
- [15] A. S. Raskin and T. W. Donnelly, Ann. Phys. (N.Y.) **191**, 78 (1989).
- [16] V. V. Frolov *et al.*, Phys. Rev. Lett. **82**, 45 (1999).
- [17] L. Tiator *et al.*, nucl-th/0012046.
- [18] C. Mertz *et al.*, Phys. Rev. Lett. **86**, 2963 (2001).
- [19] F. Kalleicher *et al.*, Z. Phys. A **359**, 201 (1997).
- [20] T. Pospischil *et al.*, Phys. Rev. Lett. **86**, 2959 (2001).
- [21] M. Warns *et al.*, Z. Phys. C **45**, 627 (1990).
- [22] I. G. Aznauryan, Z. Phys. A **346**, 297 (1993).